Science Advances
AAAS

advances.sciencemag.org/cgi/content/full/6/18/eaaz8985/DC1

Supplementary Materials for

Supramolecular prodrug hydrogelator as an immune booster for checkpoint blocker–based immunotherapy

Feihu Wang, Dongqing Xu, Hao Su, Weijie Zhang, Xuanrong Sun, Maya K. Monroe, Rami W. Chakroun, Zongyuan Wang, Wenbing Dai, Richard Oh, Han Wang, Qin Fan, Fengyi Wan*, Honggang Cui*

*Corresponding author. Email: fwan1@jhu.edu (F.W.); hcui6@jhu.edu (H.C.)

Published 29 April 2020, *Sci. Adv.* **6**, eaaz8985 (2020)
DOI: 10.1126/sciadv.aaz8985

The PDF file includes:

Other Supplementary Material for this manuscript includes the following:

(available at advances.sciencemag.org/cgi/content/full/6/18/eaaz8985/DC1)

Materials

Rink Amide MBHA Resin and amino acids were obtained from AAPPTEC (Louisville, KY). Anti-PD1 antibody (cat. no. 135234) was purchased from BioLegend. Camptothecin (CPT) was purchased from Ava Chem Scientific (San Antonio, TX). Human MMP2 recombinant protein was obtained from Thermo Fisher. Cy3 NHS-ester and Cy5 NHS-ester were purchased from Lumiprobe. All other chemicals were purchased from Sigma-Aldrich and were used without any further purification.

Cell lines

GL-261-luc brain cancer cell line and CT 26 colon cancer cell line were generously donated by M. Lim and F. Juan at The Johns Hopkins University School of Medicine, respectively. GL-261-luc cells were grown in DMEM (Gibco, Invitrogen) supplemented with 10% FBS, 100 Units/mL penicillin G sodium, 100 μg/mL streptomycin sulfate, and 100 μg/ml of G418 (Invitrogen). CT 26 cells were grown in RPMI 1640 (Gibco, Invitrogen) supplemented with 10% FBS, 100 Units/mL penicillin G sodium, and 100 μg/mL streptomycin sulfate.

Cytotoxicity assay

GL-261 cells (2.5×10^3 cells/well) were incubated in a 96-well plate overnight. The cells were then treated with varying concentrations of CPT, diCPT-PLGLAG-iRGD or P-NT solutions, with untreated cells used as a control. At scheduled time points, cell viability was tested using an MTT assay. The percentage of cell viability was calculated as follows: Cell Viability (%) = A570sample/A570control × 100%. IC_{50} values of the drug formulations were analyzed using Graph Pad Prism 5.

Inhibition of tumor spheroids

GL-261 cells were seeded at a density of 1×10^4 cells/well into agarose coated 48-well plates. After seven days, the spheroids were treated with free CPT and P-NT at the CPT concentration of 5 μM. The tumor spheroids were photographed every two days. Growth inhibition was evaluated by measuring the size of the tumor spheroids. Volume of the tumor spheroids was calculated using the equation $V= (\pi\times d_{max}\times d_{min})/6$, with d_{max} and d_{min} representing the maximum and minimum diameter of the spheroid, respectively.

Rheological Analysis

Rheological experiments were carried out on a horizontal rheometer (AR1500, TA Instruments, USA) with a controlled hydrated atmosphere at 37°C. Real time gelling was assessed by loading

the 100 µL of P-NT solution between the plates. A time sweep with constant strain of 1% and 10 Hz frequency was conducted. At 180 s, ~10 µL of 10X PBS solution was injected into the solution using a 31G insulin syringe. The gel formation kinetics was assessed by changes in storage modulus (G') and loss modulus (G") as a function of time.

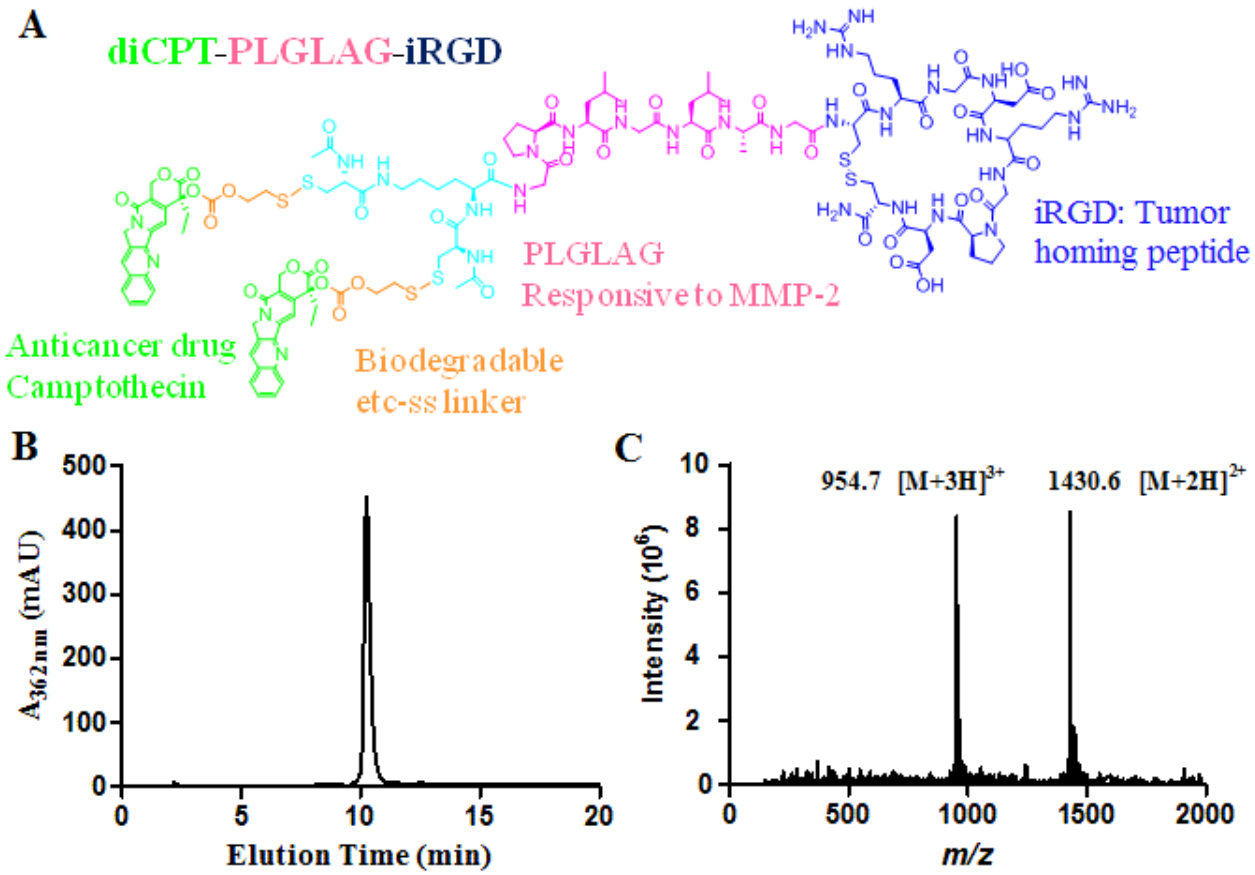

Fig. S1. Characterization of the diCPT-PLGLAG-iRGD amphiphile. (A) Chemical structure of the diCPT-PLGLAG-iRGD amphiphile. (B) RP-HPLC trace and (C) ESI MS profile of the diCPT-PLGLAG-iRGD conjugate showing high purity and the expected molecular mass, respectively.

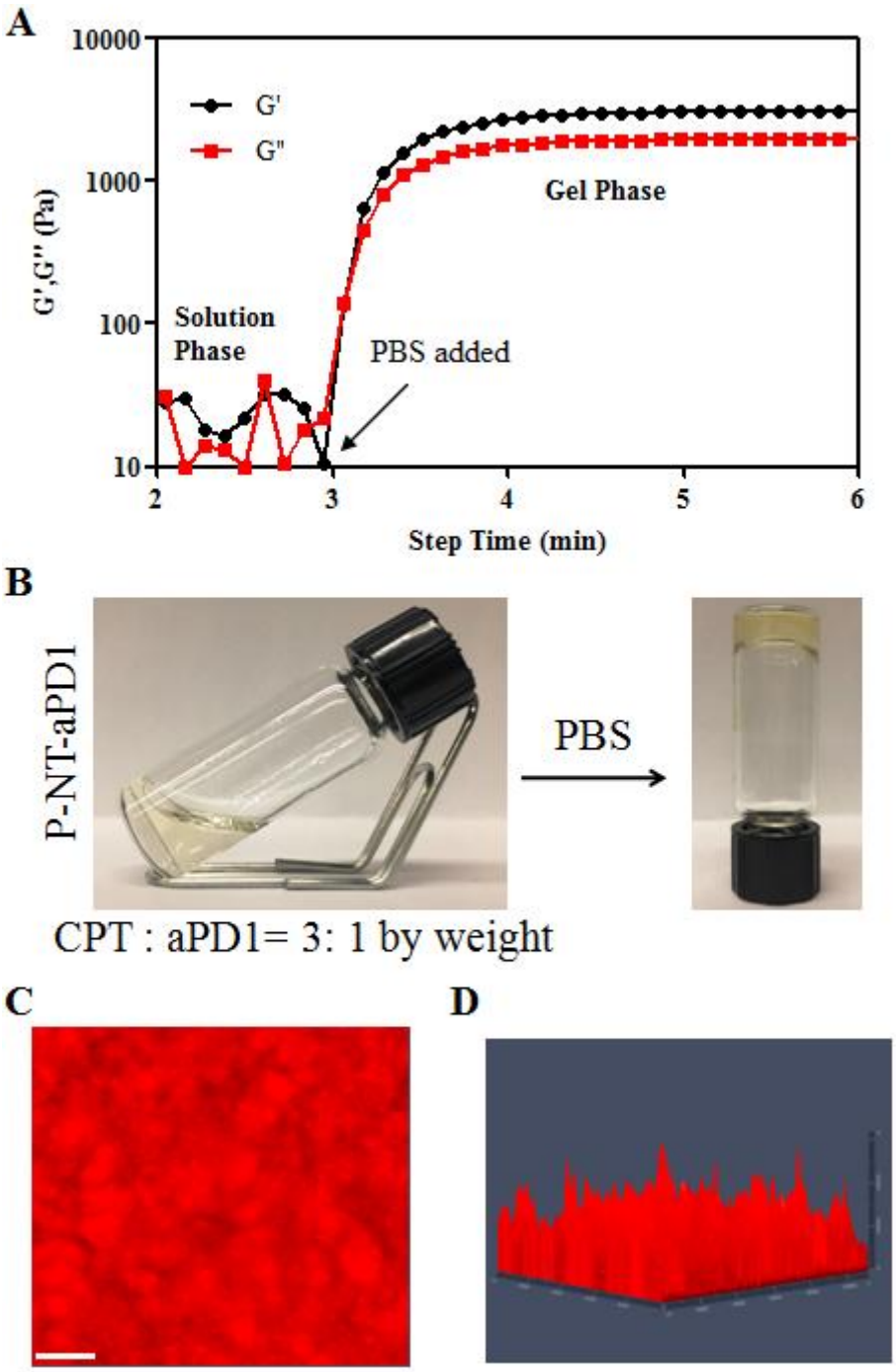

Fig. S2. Characterization of *in situ* formed P-NT and P-NT-aPD1 hydrogels. (A) Storage modulus (G') and loss modulus (G") of P-NT solution as a function of time. The rheological properties were assessed as the P-NT solution transitioned to a hydrogel upon addition of 10X PBS at 180 s. (B) Pictures of the formation of aPD1 loaded hydrogel. (C) Representative confocal 2D and (D) 2.5D images of a cryosection of P-NT-aPD1 hydrogel. aPD1 was labeled with Cy 3. Scale bar: 200 μm. Photo credit: Feihu Wang, Johns Hopkins University.

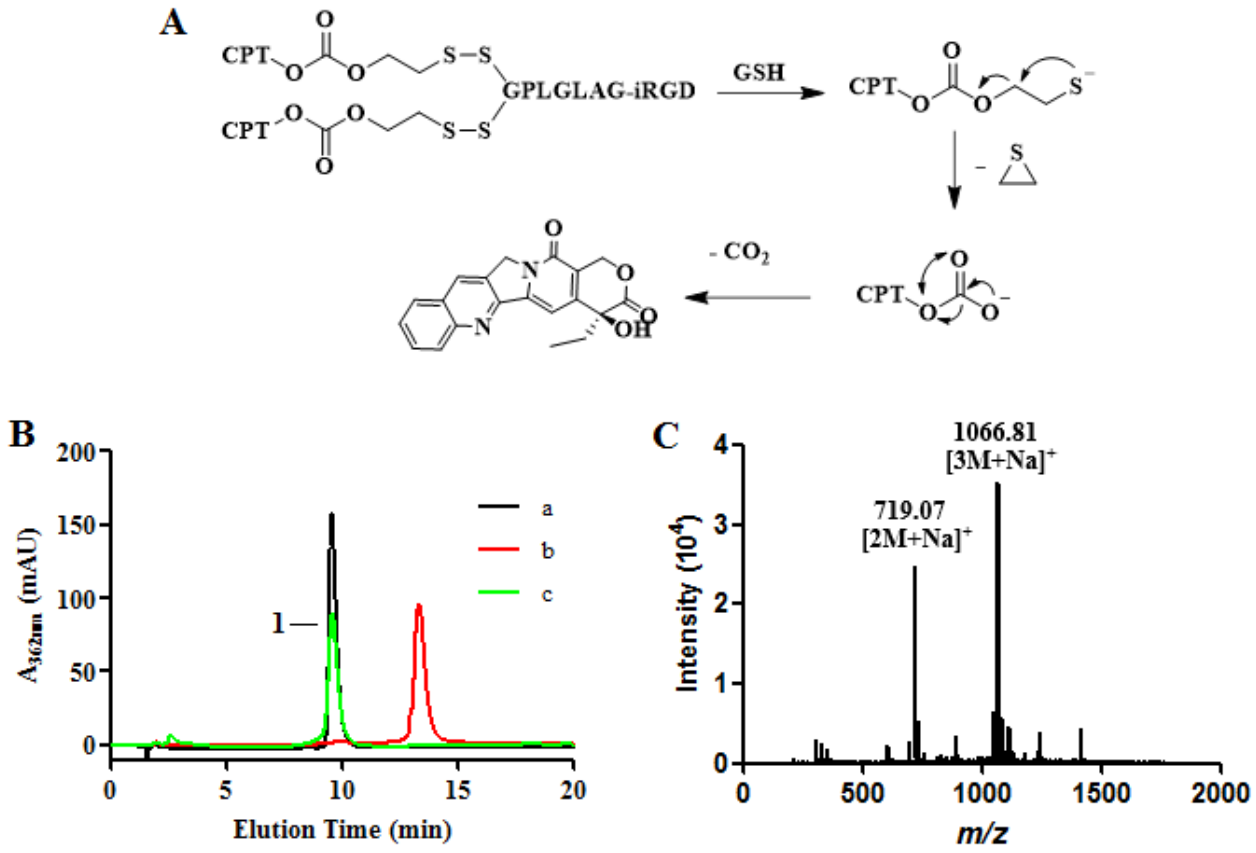

Fig. S3. GSH induced release of CPT from diCPT-PLGLAG-iRGD amphiphile. (A) Mechanism of GSH induced release of CPT from the diCPT-PLGLAG-iRGD amphiphile. (B) HPLC profile of (a) CPT, (b) diCPT-PLGLAG-iRGD and (c) diCPT-PLGLAG-iRGD with 10 mM GSH after 1 hour at 37 ℃. (C) ESI-MS spectra of peak 1 (labeled in Fig S1E) showing the exacted molecular mass with CPT.

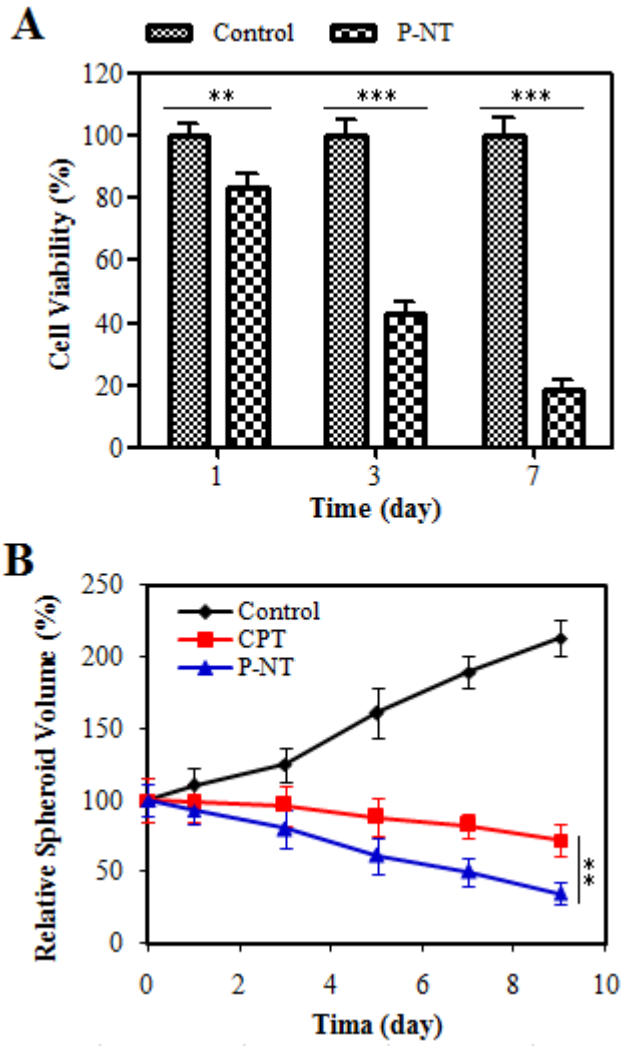

Fig. S4. *In vitro* tumor growth inhibition assays of P-NT hydrogel. (A) *In vitro* cytotoxicity of P-NT hydrogel towards GL-261 brain cancer cells. (B) Volume of tumor spheroids treated with different formulations compared with volume at day 0.

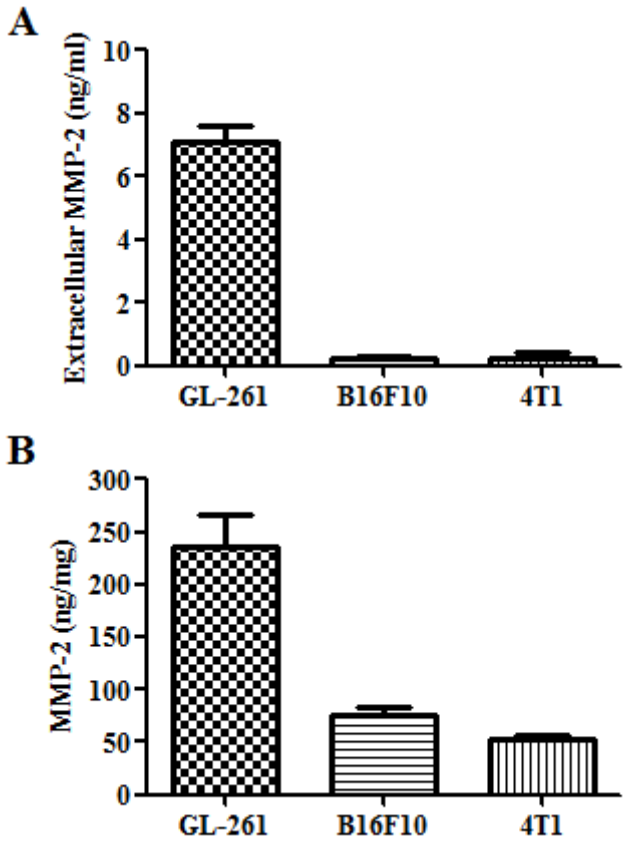

Fig. S5. The expression of MMP-2 in different tumor types. (A) ELISA was performed to detect the MMP-2 concentration in the original cell media (without further concentration of the media). (B) To determine the MMP-2 levels in tumors, tissues were collected and homogenized in PBS containing 0.5% Triton X-100. The homogenates were analyzed by ELISA and normalized by the concentration of the total protein.

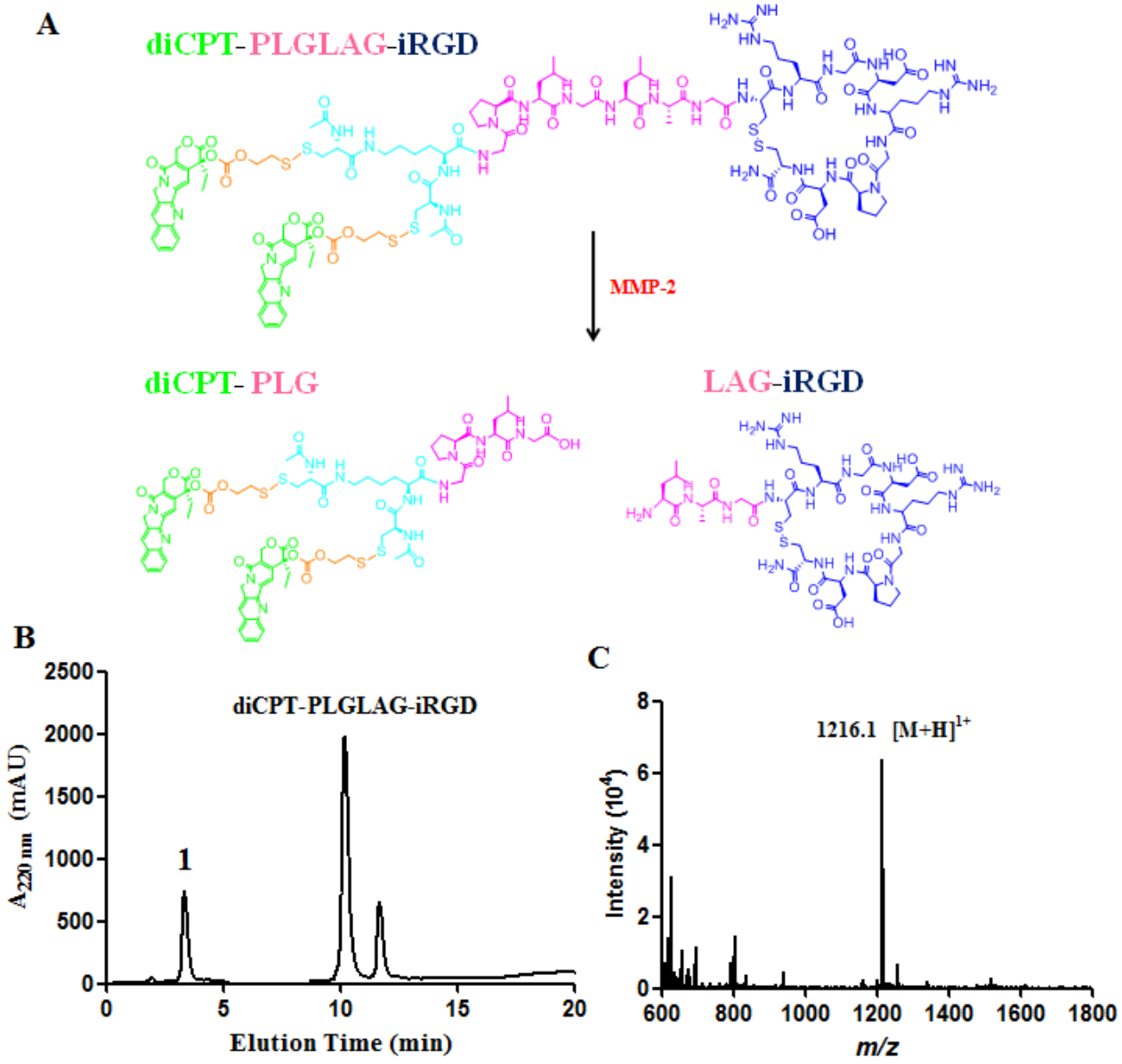

Fig. S6. MMP-2 induced cleavage of diCPT-PLGLAG-iRGD. (A) Mechanism of MMP-2 induced cleavage of diCPT-PLGLAG-iRGD. (B) HPLC analysis of diCPT-PLGLAG-iRGD solution incubated with MMP-2. (C) ESI-MS profile of peak 1 (labeled in Fig S4B) showing the exacted molecular mass with LAG-iRGD.

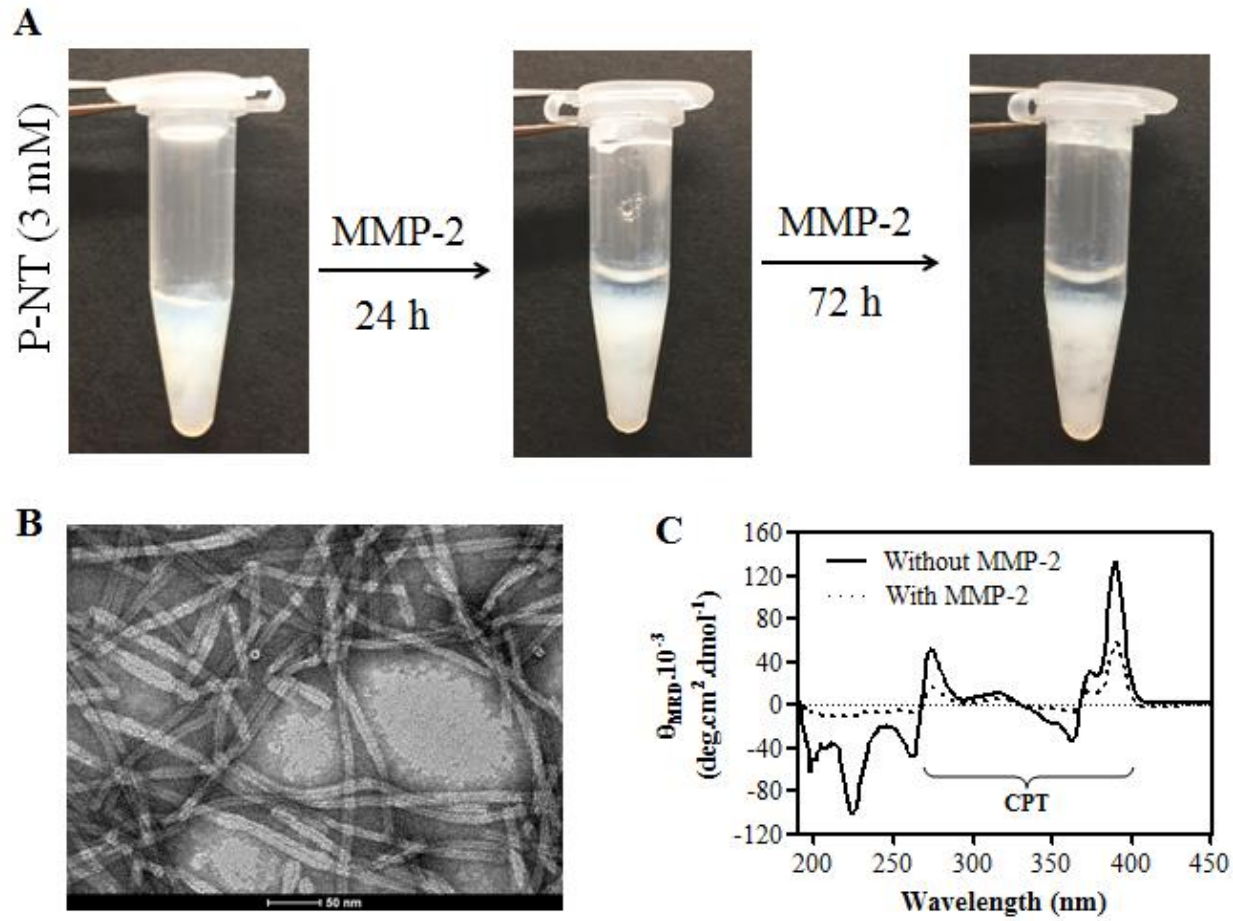

Fig. S7. MMP-2 responsive degradation of P-NT hydrogel. (A) Representative pictures of the degradation of P-NT hydrogel in the presence of MMP-2. (B) Representative TEM images of P-NTs following treatment with MMP-2. Scale bar 50 nm. (C) Circular dichroism (CD) spectra of the P-NTs treated with or without MMP-2. Photo credit: Feihu Wang, Johns Hopkins University.

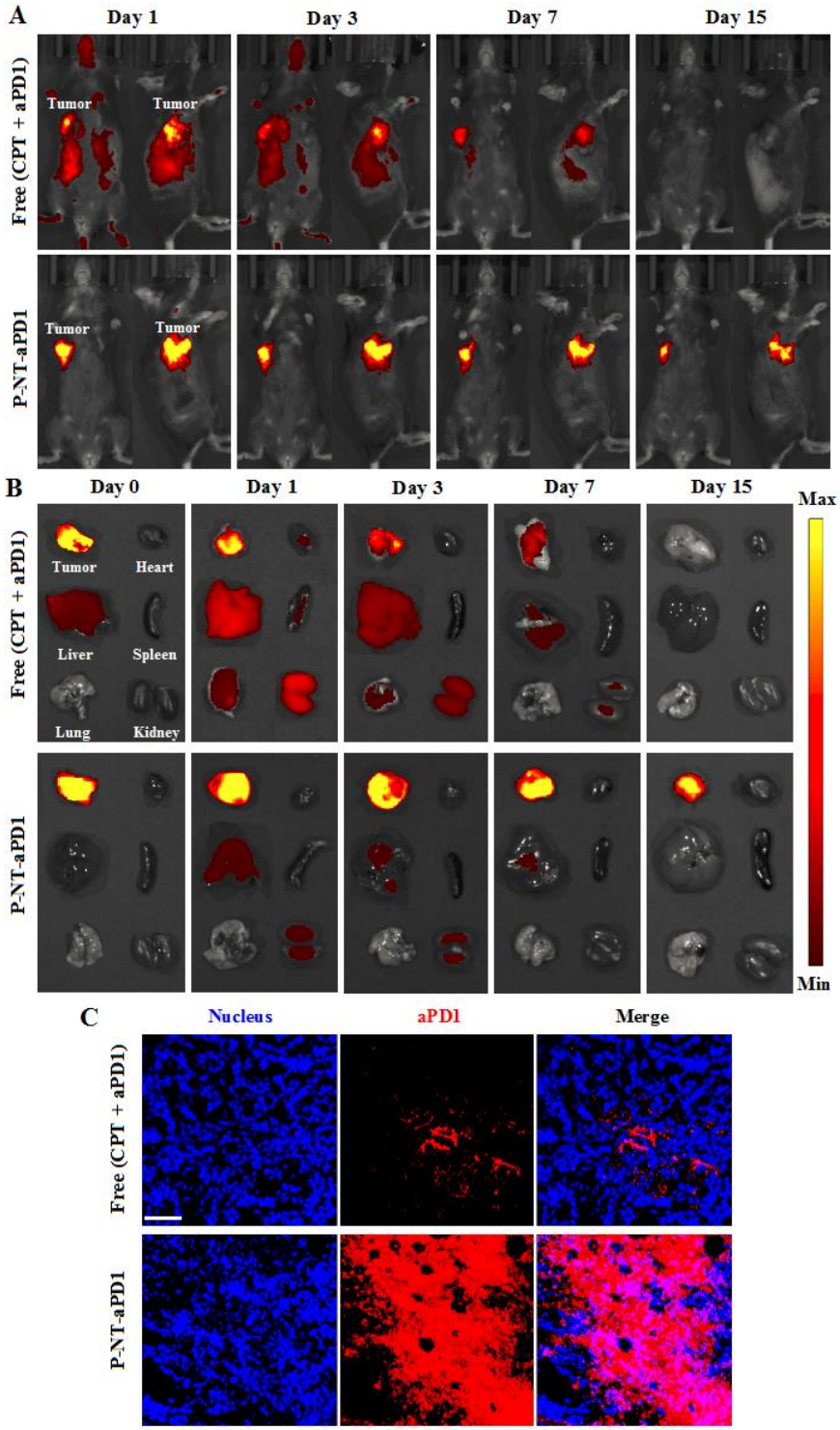

Fig. S8. Distribution of aPD1 following local administration either in solution or as a P-NT-aPD1 hydrogel. (A) Fluorescence IVIS imaging depicting the *in vivo* distribution of aPD1-Cy5.5 following local administration either in solution or as a P-NT-aPD1 hydrogel. (B) Fluorescence imaging of major tissues from GL-261 brain tumor-bearing mice that locally received either free (CPT + aPD1) or P-NT-aPD1. aPD1 was labeled with Cy 5.5. (C) Fluorescence imaging of tumor sections from GL-261 brain tumor-bearing mice that locally received either free (CPT + aPD1) or P-NT-aPD1. Red: Cy3 labeled aPD1, Blue: DAPI stained nuclei. Scale bar 200 μm.

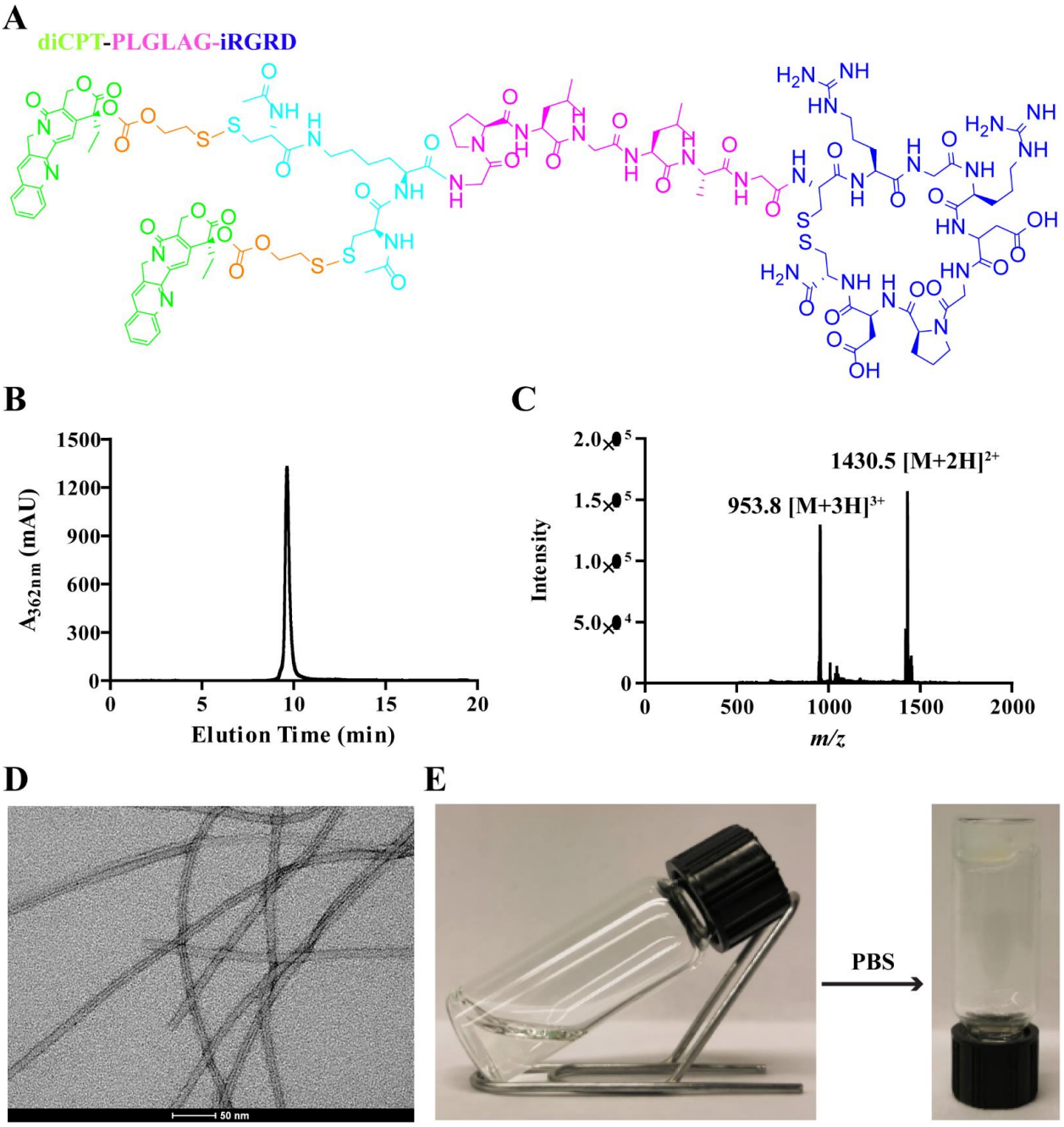

Fig. S9. Characterization of the designed diCPT-PLGLAG-iRGRD amphiphile. Here, iRGRD (cyl[CRGRDGPDC]) peptide was used as control for the iRGD (cyl[CRGDRGPDC]) peptide, which has the same amino acid composition but differs in sequences. (A) Chemical structure of the diCPT-PLGLAG-iRGRD amphiphile. (B) RP-HPLC trace and (C) ESI MS profile of conjugate diCPT-PLGLAG-iRGRD showing high purity and the expected molecular weight. (D) Representative TEM images of diCPT-PLGLAG-iRGRD nanotubes. Scale bar 50 nm. (E) Pictures of the solution-to-hydrogel transition of diCPT-PLGLAG-iRGRD nanotubes after adding PBS. Photo credit: Feihu Wang, Johns Hopkins University.

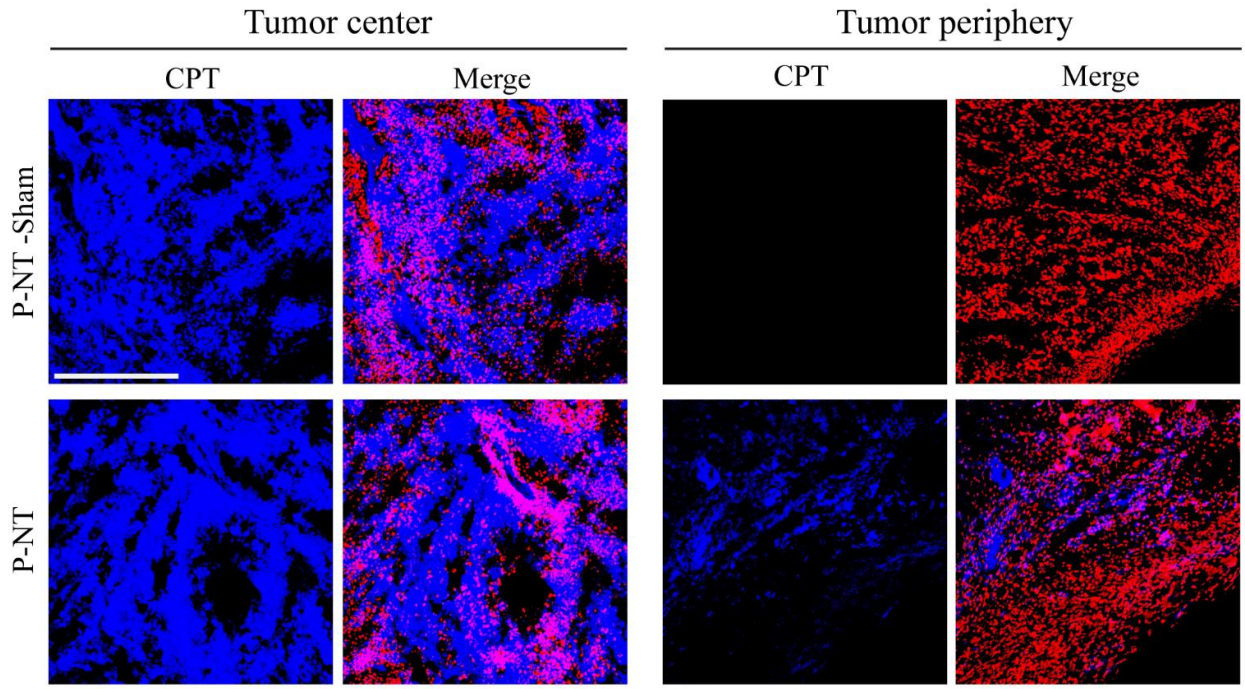

Fig. S10. Fluorescence imaging of tumor sections of GL-261 brain tumor-bearing mice after tumoral injections of P-NT-Sham (NTs formed from diCPT-PLGLAG-iRGRD) or P-NT. The images were obtained on day 3 day after treatment. Blue: CPT (Excitation at 365 nm), Red: DRAQ5TM stained nuclei, scale bar 500 μm.

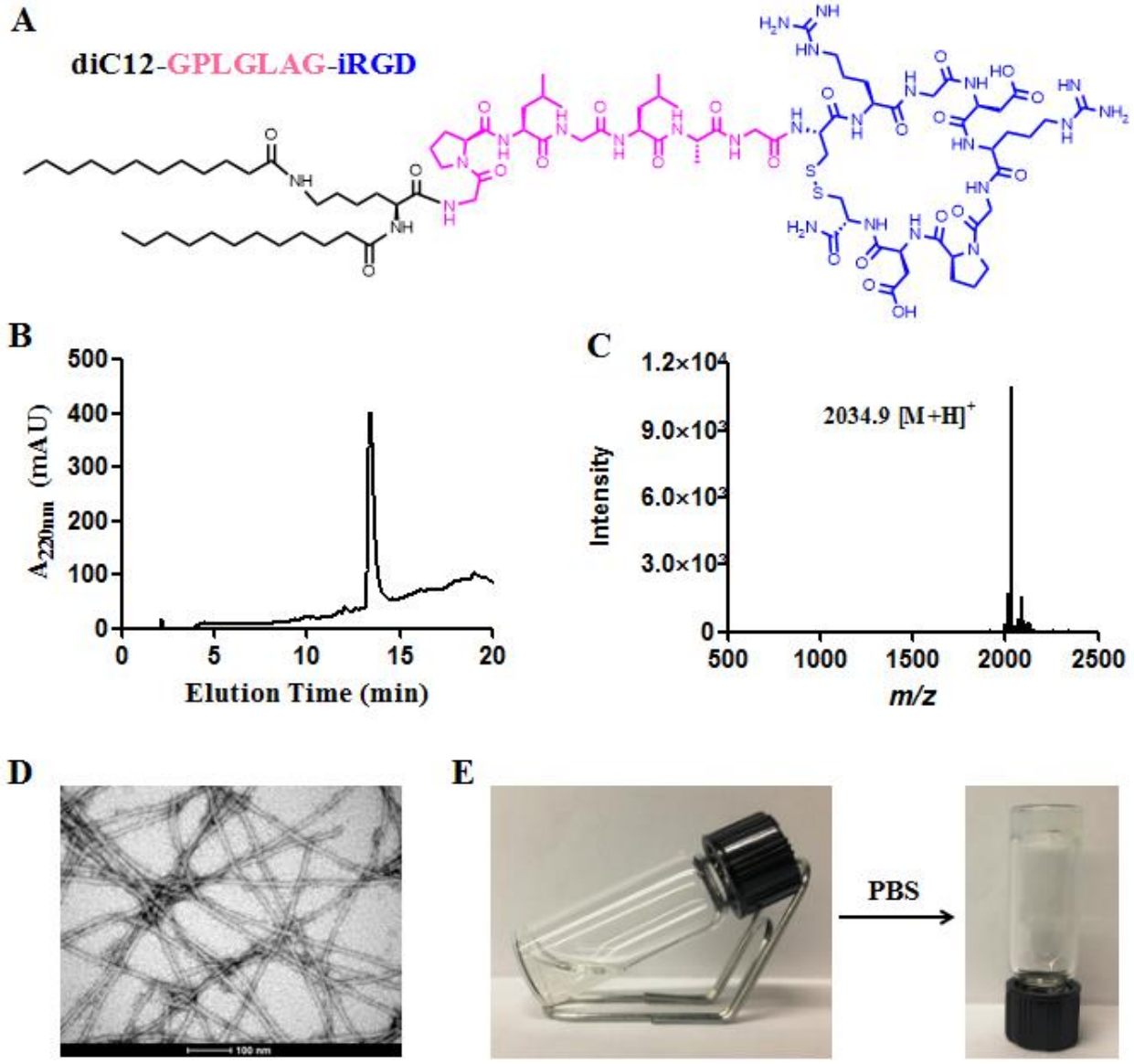

Fig. S11. Characterization of the designed diC_{12}-PLGLAG-iRGD as an *in situ* formed, drug-free hydrogel. (A) Chemical structure of the diC_{12}-PLGLAG-iRGD amphiphile. (B) RP-HPLC trace and (C) ESI MS profile of the diC_{12}-PLGLAG-iRGD conjugate showing high purity and the expected molecular mass. (D) Representative TEM images of diC_{12}-PLGLAG-iRGD nanofilaments. Scale bar 100 nm. (E) Pictures of the solution to hydrogel transition of diC_{12}-PLGLAG-iRGD nanofilaments with the addition of PBS. Photo credit: Feihu Wang, Johns Hopkins University.

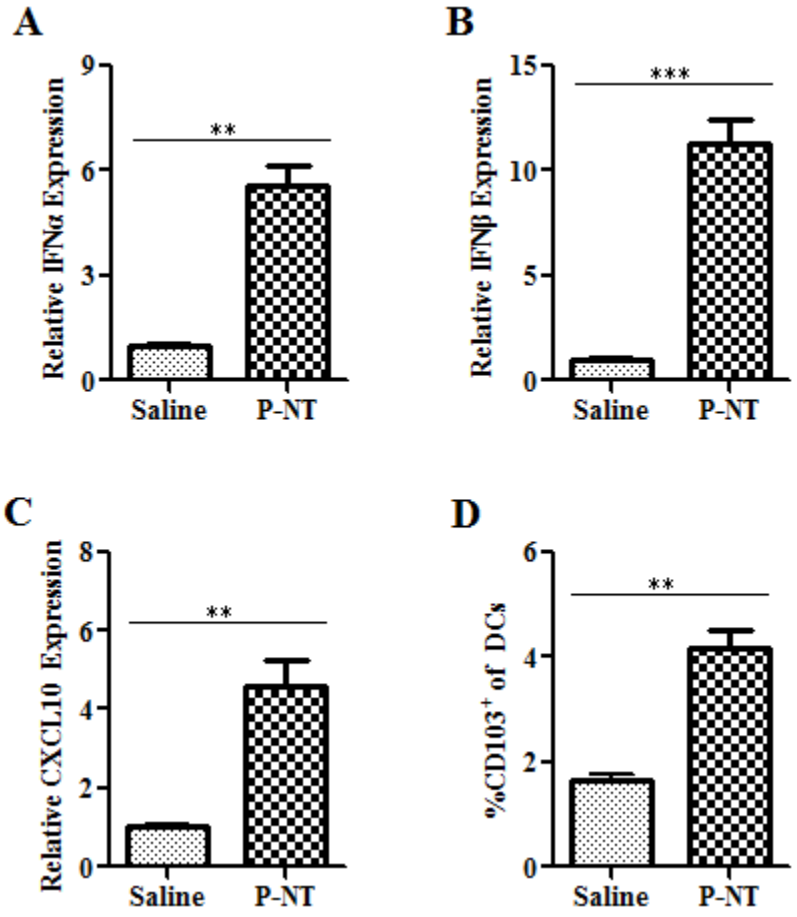

Fig. S12. The expression of type I IFNs and chemokine within the tumor tissues after different treatments. (A) Relative IFNα, (B) IFNβ and (C) CXCL10 chemokine expression in tumor tissue after 3 days of P-NT treatment. (D) Quantification of $CD103^+$ DCs within the C57BL/6 mice-bearing GL-261 tumors at day 3 post-treatment. Statistical significance was determined using a two-sided unpaired t-test. Data are given as mean ± SD (n = 3). **P ≤ 0.01, ***P ≤ 0.001.

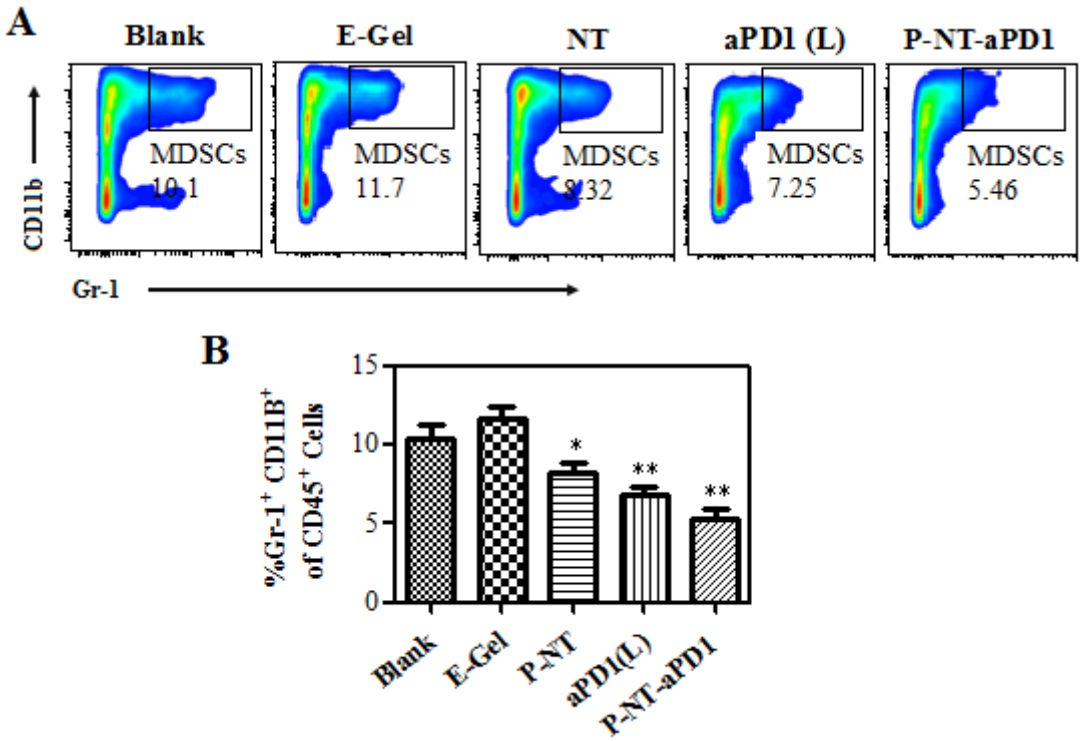

Fig. S13. Flow cytometric analysis of MDSCs. (A) Representative flow cytometric analysis images and (B) corresponding quantification of MDSCs ($Gr\text{-}1^{+}CD11b^{+}CD45^{+}$ cells) infiltration within the tumors derived from the indicated treatment groups. Data are given as mean ± SD. *P ≤ 0.05, **P ≤ 0.01.

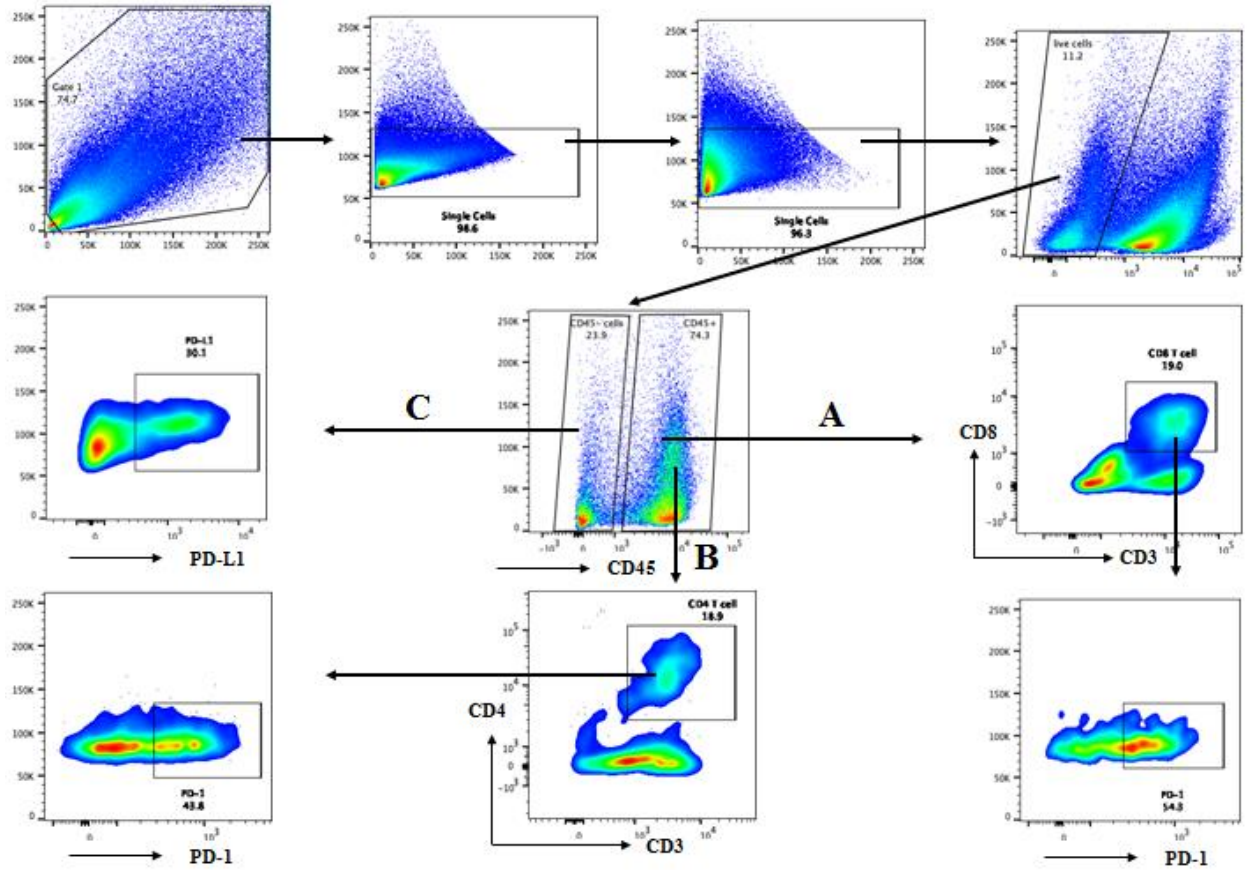

Fig. S14. Gating strategies for flow cytometric analysis of PD-1 and PD-L1 expressing cells within the GL-261 brain tumors. L/D staining was firstly used to exclude dead cells, then, lymphocyte gate was used to filter $CD45^+$ cells. (A) Analysis of PD-1 expressing CD8 T cells. CD8 T cells ($CD3^+CD8^+$) were gated from $CD45^+$ live cells. Then we identified the percentage of $PD\text{-}1^+$ cells among CD8 T cells. (B) Analysis of PD-1 expressing CD4 T cells. CD4 T cells are identified with CD4 and CD3 antibodies on the gate of $CD45^+$ cells. Gating on CD4 T cells, we identified the percentage of CD4 cells that are $PD\text{-}1^+$. (C) Analysis of PD-L1 expressing $CD45^-$ cells. Gating on $CD45^-$ cells, we identified the percentage of $CD45^-$ cells that are $PD\text{-}L1^+$.

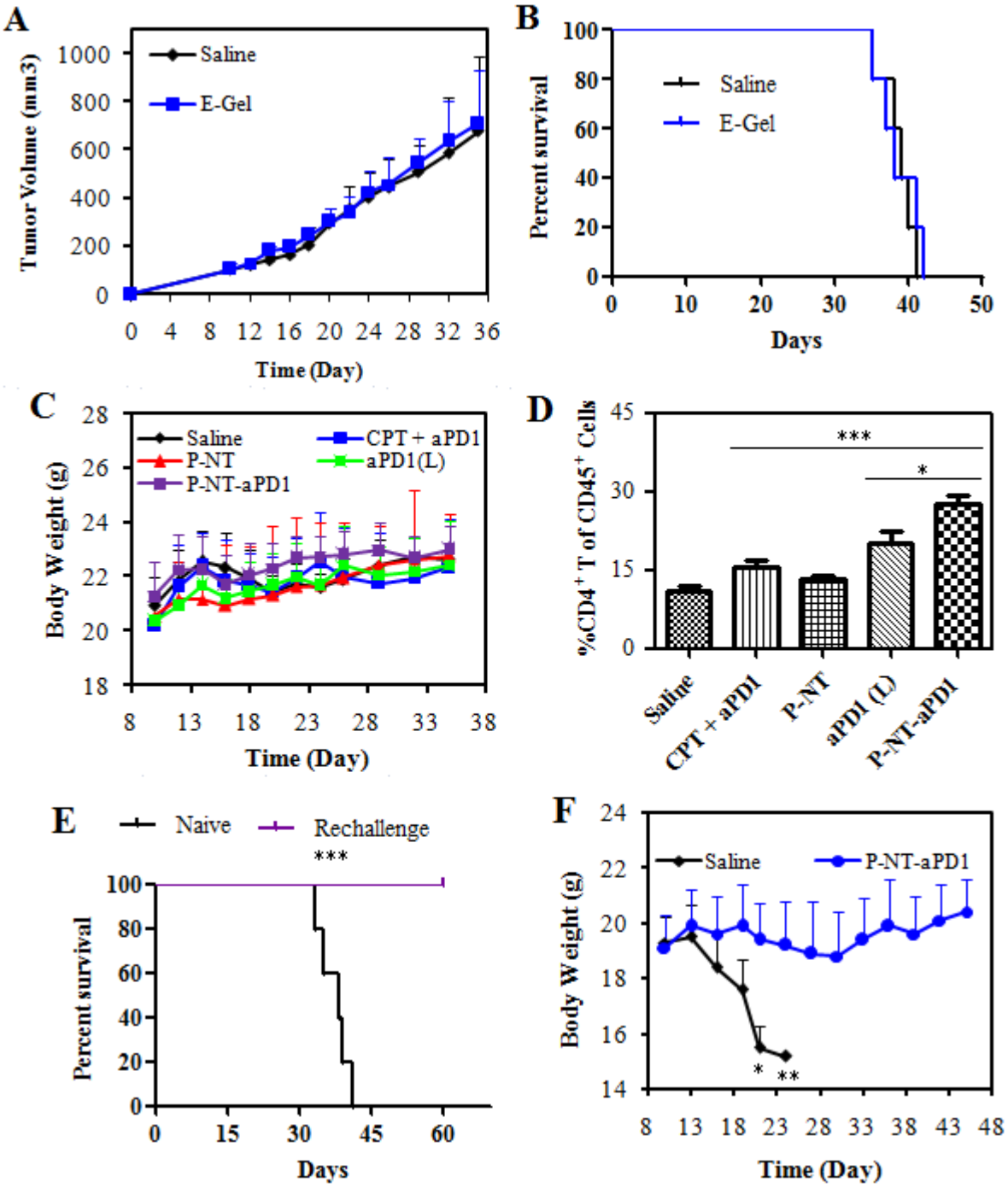

Fig. S15. Characteristics of tumor bearing mice after different treatments. (A) Tumor growth kinetics and (B) survival curves of GL-261 tumor bearing mice treated with saline or empty hydrogel (E-Gel). CPT-free diC_{12}-PLGLAG-iRGD hydrogel was used as the E-Gel. No statistical difference was detected between groups by using a two-sided unpaired t-test. (C) Body weight changes of mice in different treatment groups. (D) Quantification of $CD4^+$ T cell infiltration within tumors of different treatment groups. (E) Survival curves for naive and P-NT-aPD1 treated, rechallenged mice. Statistical significance was calculated via the log-rank (Mantel-Cox) test. ***P ≤ 0.001. (F) Body weight changes of intracranial glioma bearing mice in different treatment groups. Curves were plotted until the first mouse died. Data are given as mean ± SD. *P ≤ 0.05, **P ≤ 0.01, ***P ≤ 0.001.

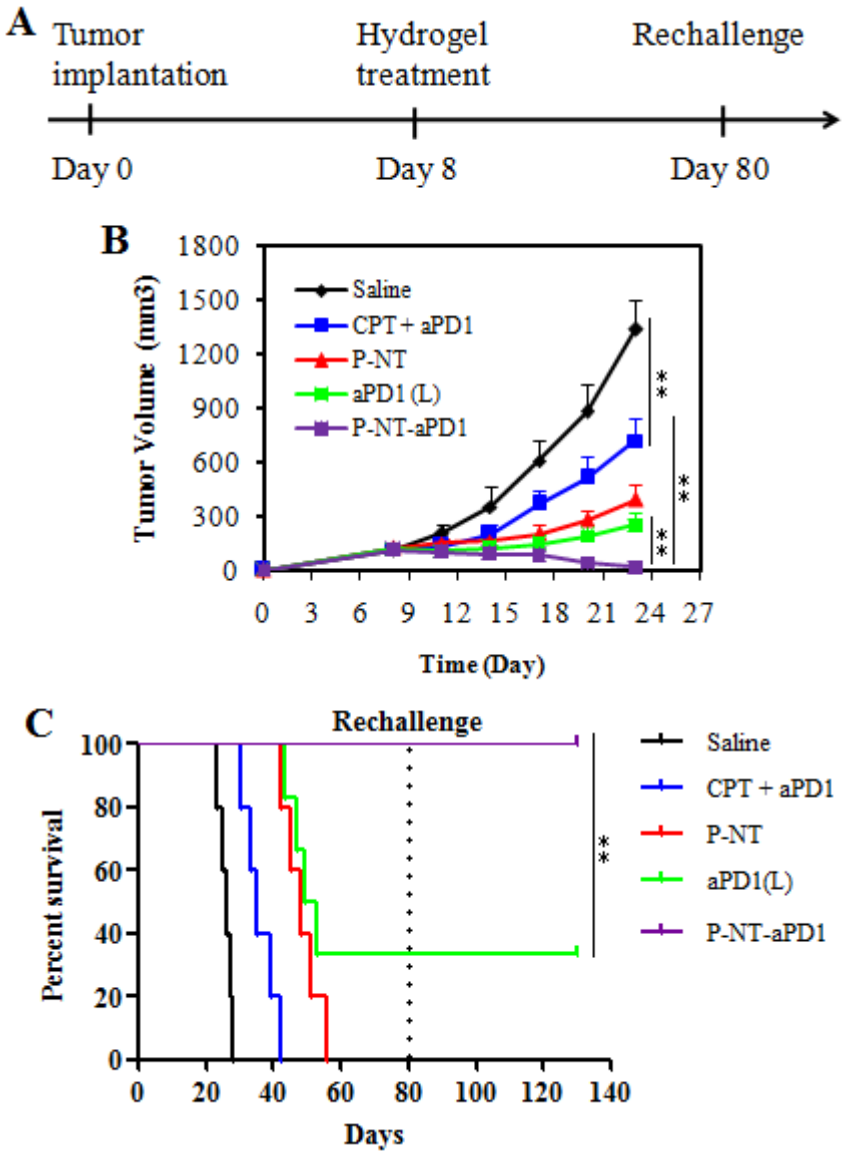

Fig. S16. Local delivery of P-NT-aPD1 hydrogels elicits regression of established CT 26 colon tumors. (A) Experimental schedule : 5×10^5 CT 26 colon cancer cells were implanted into the right flanks of BALB/c mice on day 0. Eight days later, mice were intratumorally (it.) injected with free (CPT + aPD1), P-NT, aPD1 loaded diC_{12}-PLGLAG-iRGD (aPD1-L), or P-NT-aPD1 (50 μg aPD1 per mouse; 150 μg CPT per mouse). Mice with long term survival from all treatment groups were rechallenged on the opposite flank to develop new tumors on day 80. (B) Average tumor growth kinetics of the different treatment groups. (n=8 for P-NT-aPD1 treated group, n=6 for the other groups). Growth curves were plotted until the first mouse died. Data are given as mean ± SD. **P ≤ 0.01. (C) Survival curves corresponding to the different treatment groups. Statistical significance was calculated via the log-rank (Mantel-Cox) test. **P ≤ 0.01.

Table S1. P-NT-aPD1 hydrogel had no significant effect on complete blood cell count and serum biochemistry. C57BL/6 mice were sacrificed on day 15 after P-NT-aPD1 treatment. Untreated healthy mice were used as a control. Complete blood cell counts data including: RBC, WBC, PLT, HGB and HCT. Serum biochemistry data including: ALP, ALT, AST, BUN and CRE. Data are presented as mean ± SD (n=3). Reference ranges of hematology data of healthy C57BL/6 mice were obtained from Charles River Laboratories.

	RBC (M/uL)	WBC (K/uL)	PLT (K/uL)	HGB (g/dL)	HCT (%)
Reference range	7.35-11.50	3.90-13.94	545-1849	10.9-18.1	37.2-58.0
Healthy control	10.27±0.33	8.44±2.58	1023±73	14.8±1.1	48.5±3.9
P-NT-aPD1	9.45±0.56	9.69±1.45	895±56	13.2±0.6	50.3±2.4

	ALP (U/L)	ALT (U/L)	AST (U/L)	BUN (mg/dL)	CRE (mg/dL)
Reference range	105-370	27-195	43-397	5-26	0.2-0.5
Healthy control	176±38	93±19	125±14	18.7±1.8	0.3±0.1
P-NT-aPD1	197±23	78±29	103±26	20.4±1.3	0.4±0.1